Research Square

Preprints are preliminary reports that have not undergone peer review.
They should not be considered conclusive, used to inform clinical practice,
or referenced by the media as validated information.

A realistic model of resting-state BOLD spectra in white matter

John C. Gore

john.gore@vanderbilt.edu

Vanderbilt University, Vanderbilt University

Tzu-Wei Li

Vanderbilt University, Vanderbilt University

Muwei Li

Vanderbilt University, Vanderbilt University

Warren W. Boschen

Vanderbilt University, Vanderbilt University

Kurt Schilling

Vanderbilt University, Vanderbilt University

Adam W. Anderson

Vanderbilt University, Vanderbilt University

Zhaohua Ding

Vanderbilt University, Vanderbilt University

Yurui Gao

Vanderbilt University, Vanderbilt University

Article

Keywords: Functional MRI, Hemodynamic response function, White matter, Resting-state spectrum, Shot noise, Initial dip

Posted Date: November 12th, 2026

DOI: https://doi.org/10.21203/rs.3.rs-11473671/v1

License: This work is licensed under a Creative Commons Attribution 4.0 International License.
Read Full License

Additional Declarations: No competing interests reported.

Abstract

Resting-state BOLD signals in white matter show a spectral elevation near 0.06 Hz on an exponentially decaying background, and white-matter hemodynamic response functions (HRFs) have a prominent initial dip. We model the resting signal as shot noise: randomly timed neural events are filtered by the HRF, so that the spectrum is the input spectrum multiplied by the squared HRF gain, plus instrumental noise. The initial dip and post-stimulus undershoot remove low-frequency power, making the white-matter HRF a band-pass filter with maximum gain near 0.05 Hz. One set of physiological parameters fits both a measured white-matter HRF ($R^2 = 0.993$) and the group-mean white-matter spectrum ($R^2 = 0.987$), with a resting transit time of about 4 s and a metabolic response weighted about twice as heavily as in gray matter. Deepening the dip raises the filter gain and moves its maximum toward 0.06 Hz, linking the dip to the spectral feature. A narrower line in individual spectra is reproduced either by an underdamped HRF that matches the measured response over its first 20 s or by a rhythmic input near 0.06 Hz. The model identifies which HRF properties could explain the decline of the peak with age.

Introduction

Separate analyses of the BOLD effect in white matter have recently been reported. Wu et al. [1] show that the resting-state amplitude spectrum contains a reproducible spectral peak near 0.06 Hz superimposed on an aperiodic background, confirming an earlier observation by Li et al. [2]. Schilling et al. [3] and Li et al. [4] showed that the white-matter event-related hemodynamic response function (HRF) has a delayed onset, reduced amplitude, and a more pronounced negative initial dip than the gray-matter HRF. Gao et al. [5], examining a set of normal brains, show that across white-matter bundles the depth of that dip, the height of the spectral peak, and the fractional amplitude of low-frequency fluctuations (fALFF) all covary with one another and with myelin content. Here, using numerical fitting and a recently derived, exactly solvable formulation of the HRF from a revised balloon model [6], we show that these findings follow largely from the shape of the white-matter HRF, through which all neural input is filtered: its initial dip and undershoot make it a band-pass filter, and the depth of the dip governs both the gain and the frequency of the filter maximum.

Wu et al. [1] estimated amplitude spectra of resting-state BOLD signals in white matter from 120 Human Connectome Project subjects (TR = 0.72 s) and fitted them over 0.01–0.20 Hz with a broadband floor, an exponentially decaying background and a Lorentzian line:

$$\mathcal{A}(f) = c + a\, e^{-b|f|} + \frac{A}{\pi}\,\frac{\gamma}{(f - f_0)^2 + \gamma^2} \quad (1)$$

Across subjects the median parameters are $c = 0.904$, $a = 2.65$, $b = 47.2\ \mathrm{s}$, $A = 0.0561$, $f_0 = 0.0602\ \mathrm{Hz}$ and $\gamma = 0.0150\ \mathrm{Hz}$, giving a quality factor $Q = f_0/2\gamma \approx 2.0$ ([1], Table 1). The group-mean spectrum is less peaked. Fitting Eq. (1) to it (Fig. 1B) gives $c = 0.892$, $a = 2.53$, $b = 43.2\ \mathrm{s}$, $A = 0.0769$, $f_0 = 0.0576\ \mathrm{Hz}$ and $\gamma = 0.0241\ \mathrm{Hz}$ ($Q \approx 1.2$; $R^2 = 0.9996$), and its

maximum rises only 0.10 above the preceding trough. The first two terms of Eq. (1) describe a broadband floor and an exponentially decaying shoulder; the third describes the elevation near 0.06 Hz. Below we aim to provide a mechanism for these features.

Gore et al. [6] rewrite the Buxton–Obata balloon model [7, 8] in terms of vascular transit time and venous mechanics rather than Grubb's empirical flow–volume exponent [9], linearize the resulting equations about resting values, and solve them exactly by Laplace transform. Allowing an increase in metabolism to lead the blood flow response by a delay Δ produces the dip, with closed-form depth proportional to $1 - e^{-\Delta/\tau_0}$ (where τ_0 is a resting mean transit time). The complete HRF is found to comprise an exact sum of decaying exponentials with a flow-autoregulation control that is a second-order, damped linear oscillator whose frequency and damping depend on two intrinsic physiological rate constants.

Gao et al. [5] analyzed 160 structurally defined white-matter bundles using resting-state fMRI from 120 Human Connectome Project subjects, and fitted a balloon model HRF in which a neural drive causes changes in CMRO$_2$ and CBF with a relative delay Δ. The fitted Δ correlated strongly with the isolated ~ 0.06 Hz spectral peak height ($r = 0.92,\ P < 0.001$) and with fALFF ($r = 0.75,\ P < 0.001$); the peak height itself correlated with fALFF ($r = 0.83,\ P < 0.001$); and the reconstructed HRF's initial-dip height and width both correlated with fALFF ($r = 0.74$ and $r = 0.72$, both $P < 0.001$). Association bundles showed longer fitted delays, deeper and wider dips, taller spectral peaks, and higher fALFF than projection bundles. These findings agree qualitatively with Schilling et al. [3] and Li et al. [4], who report that white-matter HRFs, relative to gray matter, have lower peak height, longer time-to-peak, and larger negative dip area.

The rest of this paper connects these findings. We first describe the resting-state signal as a shot-noise process filtered by the HRF and give its spectrum, show that the neural input alone cannot produce the elevation near 0.06 Hz, and show that the measured white-matter HRF is a band-pass filter. We then fit one set of hemodynamic parameters jointly to the measured white-matter HRF and the group-mean spectrum, compare group-mean and individual spectra, show how the depth of the dip governs the spectral elevation, and examine which properties of the HRF most influence the peak and its decline with age.

Results

Shot noise and the amplitude spectrum

Our base model describes the resting state signal as generated by a filtered shot-noise process comprising copies of an elementary pulse $h(t)$, emitted at a mean rate ν but with intervals that vary stochastically according to Poisson statistics, and with random weights α_k,

$$x(t) = \sum_k \alpha_k h(t - t_k) \quad (2)$$

Its power spectral density follows from Campbell's and Carson's theorems [10–12],

$$S(f) = \nu \langle \alpha^2 \rangle |H(f)|^2, \;\; H(f) = \int h(t)\, e^{-i2\pi ft}\, dt \quad (3)$$

The quantity actually measured and fitted, Eq. (1), is an amplitude spectrum, $\mathcal{A}(f) = |H(f)|$. We take $h(t)$ to be a compound pulse, $h = h_{\text{drive}} \star h_R$, the convolution of a neurogenic drive pulse h_{drive} with the impulse response h_R of the hemodynamic filter, i.e. the balloon-model HRF responding to the input stimulation. We further model h_{drive} as itself comprised of two components $h_{\text{drive}} = h_c + h_a$. Every signal of neural origin, fast or slow, therefore passes through the hemodynamic filter, and the spectrum is

$$\mathcal{A}(f) = |H_c(f) + H_a(f)|\; |H_R(f)| \quad (4)$$

Instrumental noise, which does not pass through the hemodynamic response, adds in power, giving the form used for fitting below

$$\mathcal{A}_{\text{model}}(f) = \sqrt{|H_c(f) + H_a(f)|^2\, |H_R(f)|^2 + N_0} \quad (5)$$

with N_0 a single fitted constant.

The neural input before filtering

To account for the aperiodic features of the amplitude spectrum $h_c \text{and } h_a$ are taken to be two elementary pulses obtained by inverse Fourier transform of the spectral components. One is an instantaneous impulse, the other a slower, symmetric transient, a Lorentzian (or Cauchy) shape:

$$h_c(t) = c\,\delta(t), \;\; H_c(f) = c \quad (6)$$

$$h_a(t) = \frac{2ab}{b^2 + 4\pi^2 t^2}, \;\; H_a(f) = a\, e^{-b|f|} \quad (7)$$

h_c here is a single discrete “instantaneous” impulse but on the time scales of the data could also be generated by a near-synchronous local burst of short spikes.

h_a has a half-width $b/2\pi \approx 7.5$ s, too long to be the time course of a single event. However, mathematically the Cauchy pulse of Eq. (7) can be exactly represented as a continuous mixture of Gaussian kernels,

$$h_a(t) = a \int_0^\infty \mathcal{N}(t; 0, v)\;\; p_{1/2}(v; k)\;\; dv, \;\; k = \left(\frac{b}{2\pi}\right)^2 \quad (8)$$

where $\mathcal{N}(t; 0, v) = (2\pi v)^{-1/2} e^{-t^2/2v}$ is a Gaussian kernel of variance v centered at t = 0 and

$$p_{1/2}(v;k) = \sqrt{\frac{k}{2\pi}}\; v^{-3/2}\, e^{-k/2v} \quad (9)$$

is the one-sided, $1/2$-stable (Lévy) density function. Physically, equations (8)–(9) describe h_a not as the shape of a single elementary event but as a population-averaged impulse response produced by superposing many local bursts of drive, each individually a smooth (Gaussian) rise and fall, whose durations $\sqrt{v}$ are heterogeneous across the population and heavy-tailed rather than narrowly distributed: most bursts are brief, but there are a minority that last much longer. This formulation reproduces the exponential shoulder exactly.

The combined transform of the two “input” pulses is then

$$H_c(f) + H_a(f) = c + a\, e^{-b|f|} \quad (10)$$

which monotonically decreases with $|f|$ for any choice of $a, b, c > 0$. Figure 1 shows Eq. (10) evaluated at the fitted values of Eq. (1): a smooth, featureless curve. The two input components give a floor and a shoulder but cannot on their own produce the elevation near 0.06 Hz; that must come from the hemodynamic filter (see below).

The hemodynamic filter

We identify h_R with the impulse response of the revised balloon model described by Gore et al., linearized about resting values and solved by Laplace transform. Two parallel inputs are integrated for the final response. The metabolic branch, driven by oxygen consumption, has real, negative poles at $s = -1/\tau_0$ and a repeated pole at $s = -1/\tau_m$ (τ_0 the resting mean transit time, τ_m a lumped metabolic time constant) corresponding to a sum of exponential responses. A flow-autoregulation term however describes the dynamics of a vasoactive signal z and inflow f_{in},

$$\frac{dz}{dt} = \epsilon\, u(t-\Delta) - \kappa\, z - \gamma_a (f_{in} - 1), \quad \frac{df_{in}}{dt} = z \quad (11)$$

z is a vasoactive signal generated by neural activity with efficacy ϵ, decaying at rate κ and subject to autoregulatory feedback at rate γ_a; it is an intermediate quantity that converts a brief neural event into a smooth flow response. f_{in} is the input flow rate expressed relative to baseline and $u(t-\Delta)$ is a unit impulse (a brief neural event) delayed to occur at $t = \Delta$. Eq. (11) describes a damped linear oscillator with characteristic roots in the Laplace domain

$$s = -\sigma \pm i\omega_d, \;\; \sigma = \frac{\kappa}{2}, \;\; \omega_d = \sqrt{\gamma_a - \frac{\kappa^2}{4}} \quad (12)$$

This complex pair of roots describes a damped oscillator. Combining both branches, with ρ, α, τ_v, $\tau_c = \alpha\,(\tau_0 + \tau_v)$ fixed constants of the revised balloon model, the Laplace transform of the response is

$$H_R(s) = \underbrace{\frac{-G_m}{(1+\tau_m s)^2\,(1+\tau_0 s)}}_{\text{metabolic}} + G_f\, e^{-\Delta s}\, \underbrace{\frac{\rho\,(1+\tau_0 s) + (1-\alpha+\alpha\,\tau_v s)}{(s^2+\kappa\, s+\gamma_a)\,(1+\tau_c s)\,(1+\tau_0 s)}}_{\text{flow}} \quad (13)$$

with G_m, G_f overall branch gains. Here, *α* is Grubb's exponent, which sets how much venous blood volume changes for a given change in blood flow. τ_v is a venous viscoelastic time constant: how quickly the vein wall itself mechanically relaxes in response to a change in pressure or volume. $\tau_c = \alpha\,(\tau_0 + \tau_v)$ is a venous compliance time constant: the effective timescale over which venous blood volume equilibrates to a new flow level, combining the transit time τ_0 and the wall's relaxation time τ_v. ρ is a fixed dimensionless constant that depends on *α* and BOLD-signal weighting coefficients set by field strength, echo time, and baseline oxygen extraction. It fixes the relative weight of the two terms in the flow contributions.

The measured white-matter HRF has a characteristic shape. Schilling et al. [3] estimated HRFs from the resting-state data of 199 Human Connectome Project subjects by blind deconvolution [13]. Their population-averaged white-matter response has an initial dip of − 0.31 at 2.9 s, a peak of 0.72 at 7.9 s and a shallow undershoot of − 0.06 near 18 s (Fig. 2A), and the responses at the midpoints of individual tracts are almost identical (their Fig. 7). The dip is 43% of the peak, whereas in gray matter it is barely evident.

Because the dip and the undershoot have the opposite sign to the main response, they cancel part of its low-frequency content. The amplitude spectrum $|H(f)|$ of the measured HRF therefore rises from its zero-frequency value to a maximum 1.35 times higher at 0.048 Hz before falling at higher frequencies (Fig. 2B): the white-matter HRF is a band-pass filter. Without the initial dip the maximum is smaller and moves to about 0.03 Hz. By Eq. (4), a superposition of randomly timed white-matter HRFs driven by a flat input spectrum therefore has a spectral maximum near 0.05 Hz without any resonance in the flow dynamics. A direct simulation, in which Poisson-distributed events of random amplitude were convolved with the measured HRF and sampled as in the HCP data (TR = 0.72 s, 1200 frames, 120 subjects), reproduces the maximum at 0.050 Hz (Fig. 2B).

Joint fit of the HRF and the resting-state spectrum

If the resting-state spectrum arises from neural events filtered by the HRF, the same hemodynamic parameters must describe both the measured HRF and the spectrum. We therefore fitted Eq. (13), with $\tau_m,\ \tau_v,\ \alpha$ held at the values fitted by Gore et al. [6] to the canonical HRF ($\tau_m = 2.99$ s, $\tau_v = 10.03$ s, $\alpha = 0.326$), simultaneously to the white-matter HRF of Schilling et al. [3] and to the group-mean white-matter spectrum of Wu et al. [1] over 0.01–0.20 Hz, using Eq. (5) for the spectrum. The two residuals were normalized by the variance of each data set and weighted equally. The free parameters were $\tau_0,\ \kappa,\ \gamma_a,\ \Delta,\ G_m,\ G_f$, the input parameters $c,\ a,\ b$ and the noise term N_0. The fit gives

$$\tau_0 = 4.15\ \mathrm{s}, \quad \kappa = 0.540\ \mathrm{s}^{-1}, \quad \gamma_a = 0.218\ \mathrm{s}^{-2}, \quad \Delta = 2.91\ \mathrm{s}, \quad G_m/G_f = 2.35 \qquad (14)$$

with $\mathrm{R}^2 = 0.993$ for the HRF and $\mathrm{R}^2 = 0.987$ for the spectrum (Fig. 3). The transit time is about 2.4 times the value fitted to the canonical gray-matter HRF (1.70 s; [6]), consistent with lower blood flow relative to blood volume in white matter, and the metabolic branch is weighted about twice as heavily relative to the flow branch in the canonical gray-matter fit ($G_m/G_f = 1.09$; [6]), consistent with the deeper dip. The flow stage is moderately damped (damping ratio $\kappa/2\sqrt{\gamma_a} = 0.58$), so the fitted HRF does not ring, and its gain peaks at 0.047 Hz, 1.48 times its zero-frequency value. The fitted input has $b = 111$ s, so the slow bursts of Eq. (7) have a half-width of about 18 s, longer than the 7.5 s implied by Eq. (1), because the band-pass filter suppresses the lowest frequencies of the input. The instrumental noise term, $\sqrt{N_0} = 0.88$, carries the high-frequency floor. With the HRF fixed at the values fitted to the measured response alone, and only the input and noise free, the spectrum is fitted with $\mathrm{R}^2 = 0.973$.

The filtered input accounts for the elevation of the spectrum between about 0.03 and 0.08 Hz (Fig. 3A), but not for its shallow local maximum: the largest residual is 0.15 (9%) at 0.06 Hz, and the observed spectrum exceeds the model by about 2% of its amplitude integral over 0.03–0.09 Hz. For comparison, Wu et al. [1] attribute on average 11.8% of the spectral energy in this band to the Lorentzian component of Eq. (1), measured against a monotonic exponential background.

Group-mean and individual spectra

The group-mean spectrum is less peaked than individual spectra. With the per-subject mean parameters of Wu et al. [1] (Table 1) ($c = 0.893$, $a = 2.94$, $b = 51.4$ s, $A = 0.0644$, $f_0 = 0.0597$ Hz, $\gamma = 0.0153$ Hz), Eq. (1) rises 0.62 above its trough, compared with 0.10 for the group mean. Much of this difference follows from averaging as the peak frequency varies between subjects with a standard deviation of 0.012 Hz, comparable to the line width γ. Averaging 4000 spectra generated from Eq. (1) with parameters drawn from the reported means and standard deviations reduces the rise to 0.19 and reproduces the group mean with $\mathrm{R}^2 = 0.978$ (Fig. 4A).

Individual spectra therefore contain a narrower line ($Q \approx 2$) than the group mean ($Q \approx 1.2$), and a broadband input filtered by the jointly fitted HRF does not reproduce it: Eq. (5) then fits the per-subject mean spectrum with $\mathrm{R}^2 = 0.925$ and gives only a broad maximum at 0.046 Hz (Fig. 4B).

The model has many parameters, and several parameter sets may fit the spectrum comparably well. We therefore refitted all hemodynamic parameters, including τ_m, τ_v, α, jointly to the individual spectrum and the measured HRF, giving priority to the spectrum (weights 0.9 and 0.1) and using only the first 20 s of the HRF, the part that is well determined. This gives $\mathrm{R}^2 = 0.999$ for the spectrum, with a line of prominence 0.58 against 0.62 in the target, and $\mathrm{R}^2 = 0.95$ for the HRF over 0–20 s (Fig. 4B, C). Over those 20 s the fitted HRF follows the measured dip, peak and undershoot, although its dip is 0.7 s early, its peak 10% lower, and its undershoot deeper (− 0.12 against − 0.06). Its flow stage is underdamped

(damping ratio 0.22; pole $Q = 2.2$ at 0.060 Hz), and after 20 s the response rises again to a second positive lobe, 26% of the peak, at 24.5 s.

The measured HRF gives little information after 20 s. It was estimated by blind deconvolution with a double-gamma basis, which cannot produce a second positive lobe, and the reported response ends at 25 s; within the 20–25 s interval it lies close to zero and within about 0.05 of the baseline. The underdamped solution therefore cannot be excluded on the basis of the measured HRF. It does, however, require parameter values at or near the limits of the allowed ranges: a transit time of 7.8 s, no neurovascular delay (Δ = 0) and a Grubb exponent of 0.60. Across a range of weights, closer agreement with the HRF is obtained only at the expense of the spectral line: an HRF fit of $R² = 0.99$ over 0–25 s allows a spectral fit of only $R² = 0.935$, with a line of prominence 0.12 (Fig. 4D).

The narrow line can instead come from the input. Adding a Lorentzian line to the input spectrum, with the jointly fitted HRF unchanged, fits the individual spectrum with $R² = 0.999$ (line at 0.061 Hz, $Q = 2.2$; 38% of the input amplitude in 0.03–0.09 Hz) and the group mean with $R² = 0.9998$ (line at 0.061 Hz, $Q = 1.5$; 24%). The present data do not distinguish the two explanations. They differ in the HRF after about 20 s: an underdamped hemodynamic filter predicts a second positive lobe near 25 s, whereas a rhythmic input predicts none..

The initial dip and the spectral elevation are linked

Because every neural input passes through the same filter, the dip and the spectral elevation are two expressions of the same property of the HRF. Figure 5 varies the relative weight of the metabolic branch, G_m/G_f, with all other parameters at their fitted values (Eq. (14)). As the metabolic weight rises from 1.0 to 3.25, the dip deepens from 13% to 79% of the peak, the maximum gain of the filter relative to its zero-frequency value rises from 1.0 to 9.5, and the frequency of that maximum moves from zero to 0.058 Hz (Fig. 5B, C). All three change monotonically together. Whatever the input, the elevation of the spectrum near 0.05–0.06 Hz is therefore amplified most, and centered closest to 0.06 Hz, where the dip is deepest, which is the pattern reported bundle by bundle by Gao et al. [5].

The neurovascular delay Δ has a weaker and non-monotonic effect. Increasing Δ from 0.5 to 5 s deepens the dip from 3% to 58% of the peak and moves the gain maximum from 0.035 to 0.051 Hz, but the maximum gain first falls from 1.63 to 1.45 and then rises to 1.86.

Sensitivity of the spectral peak and predictions for aging

Starting from the jointly fitted HRF (Eq. (14)) and the rhythmic-input description of the per-subject mean spectrum (above), each hemodynamic parameter was varied alone and the prominence of the resulting spectral peak was measured (Fig. 6). Around the fitted values the elasticity of the peak, the percentage change in prominence per percentage change in the parameter, is − 2.3 for κ, − 1.6 for τ_0, + 1.2 for γ_a, + 0.9 for both G_m/G_f and Δ, − 0.8 for τ_m, and about + 0.2 for α and τ_v. The peak is therefore

controlled mainly by the damping of the flow stage, which κ and γ_a set together, and next by the transit time. Halving the peak requires a 34% increase in κ, a 50% increase in τ_0 or a 27% decrease in γ_a, whereas halving the metabolic weight or the delay reduces it by only about a third.

Wu et al. [1] found that the white-matter peak declines with age in the HCP-Aging cohort and has almost vanished by 81–90 years. Several age-related changes could each produce such a decline in the model: a longer transit time from reduced blood flow, blunted neurovascular coupling (a shorter-lived vasoactive signal or weaker autoregulatory feedback), and, if myelin loss lowers the metabolic weight, a smaller metabolic contribution. These possibilities make different predictions for the HRF. A longer transit time lowers the peak with little change in the dip (dip-to-peak ratio 0.42 to 0.45 for a 50% increase) but delays the time to peak (8.2 to 8.8 s). A lower metabolic weight or weaker feedback lowers the peak and makes the dip shallower. A faster-decaying vasoactive signal lowers the peak while deepening the dip (0.42 to 0.56 for a 34% increase in κ). A decline of the peak without any change in the shape of the HRF would instead indicate a weakening of the rhythmic input component, if it exists, consistent with the parallel decline of the corresponding peak in cerebrospinal fluid [1]. White-matter HRFs and spectra measured in an aging cohort could therefore identify which factor dominates.

Discussion

These results account for the white-matter resting-state spectrum as neural input passed through the white-matter HRF. Randomly timed events, brief and prolonged, produce a spectrum equal to the input spectrum multiplied by the squared gain of the HRF [10–12]. Because the initial dip and the undershoot oppose the main response, the white-matter HRF is a band-pass filter with maximum gain near 0.05 Hz, and a single set of hemodynamic parameters describes both the measured HRF and the group-mean spectrum. The parameters are physiologically plausible: a resting transit time of about 4 s, a neurovascular delay of about 3 s, and a metabolic branch weighted more heavily than in gray matter. The depth of the dip sets both the gain and the frequency of the filter maximum, which gives a mechanistic basis for the covariation of dip and spectral peak across bundles reported by Gao et al. [5], and for their shared relation to myelin content if myelination alters the balance between oxygen consumption and flow. The sensitivity analysis identifies the damping of the flow stage and the transit time as the main hemodynamic controls of the peak, and indicates how its decline with age could be attributed.

The narrower line in individual spectra has two possible origins that the present data cannot separate. An underdamped white-matter HRF, fitted with priority given to the spectrum, reproduces the line and agrees with the measured HRF over the first 20 s, but predicts a second positive lobe near 25 s, where the measured HRF is not well determined, and requires parameter values near the edge of the plausible range. Alternatively, a rhythmic component of the input near 0.06 Hz, filtered by the measured HRF, reproduces both group-mean and individual spectra. Candidate sources of such a rhythm include spontaneous vasomotion, which would enter through the flow branch, slow rhythms in neural or glial activity, and the low-frequency oscillations coupled to cerebrospinal fluid flow that show a similar

spectral peak [1, 14]. In either case the HRF determines where in frequency the line appears, and the dip how strongly it is amplified.

Several limitations and potential confounds apply. First, the spectrum and the HRF come from different HCP samples (120 and 199 subjects). Second, the HRF of Schilling et al. [3] was obtained by blind deconvolution of resting-state data with a double-gamma basis, so it is not independent of the resting-state signal, is constrained in shape and is not reported beyond 25 s; task-evoked white-matter HRFs [4] estimated without a basis constraint would provide a stronger test. Third, τ_m, τ_v, α were held at gray-matter values, and the model inherits the single-compartment and linearization assumptions of Gore et al. [6]. Fourth, non-neural signals that bypass the hemodynamic filter, such as aliased cardiac and respiratory fluctuations at the HCP sampling rate, inflow effects of cerebrospinal fluid near the ventricles, and partial-volume contamination from adjacent gray matter, could contribute power in the same band.

Methods

Data

No new data were acquired. The white-matter resting-state spectra were taken from Wu et al. [1], who estimated Welch amplitude spectra over 0.01–0.20 Hz from resting-state fMRI of 120 Human Connectome Project (HCP) subjects (TR = 0.72 s). The group-mean white-matter spectrum was resampled at 400 frequencies over 0.01–0.20 Hz. Per-subject spectra were represented by Eq. (1) with the means and standard deviations of their Table 1. The white-matter HRF was the population-averaged response of Schilling et al. [3], estimated from resting-state data of 199 HCP subjects by blind deconvolution [13] with a double-gamma basis and a temporal derivative.

Hemodynamic model

The impulse response of Eq. (13) was computed by numerical inverse Fourier transform (time step 0.02 s, window 400 s). The constant ρ = α(1 − 1/βD), with βD = 1.256 obtained from the 3 T signal constants of Gore et al. [6]. Unless stated otherwise, τm, τv and α were fixed at 2.99 s, 10.03 s and 0.326, the values fitted by Gore et al. [6] to the canonical HRF with an initial dip. All neural input passes through the filter, and instrumental noise is added in power (Eq. (5)).

Model fitting

Fits used nonlinear least squares (SciPy least_squares) with multiple random starts within bounds; the best solution is reported. Eq. (1) was fitted to the digitized group-mean spectrum with 200 starts. For joint fits, the HRF and spectral residuals were each divided by the standard deviation of their data and the square root of their number of points, multiplied by the square roots of weights w and 1 − w, and concatenated. The group-mean joint fit (Eq. (14)) used w = 0.5, with τ0, κ, γa, Δ, Gm, Gf, the input parameters c, a, b and N0 free (40 starts). For the individual spectrum, the spectrum-prioritized fit used w = 0.1, only the first 20 s of the HRF, and all nine hemodynamic parameters free within bounds (τ0 0.3–

15 s, κ 0.01–5 s^{-1}, γa 0.01–5 s^{-2}, Δ 0–8 s, τm 0.5–8 s, τv 0–30 s, α 0.2–0.6), with 80 starts. The trade-off of Fig. 4D was mapped by repeating the fit for w = 0.1 to 0.9 with the HRF to 25 s (80 starts per weight, 720 fits). The rhythmic input was represented by a Lorentzian line added to the input amplitude spectrum, with the hemodynamic parameters held at the group-mean joint fit.

Simulations and sensitivity analysis

Poisson-distributed events (rate 0.1 s^{-1}, amplitudes drawn from a normal distribution with mean 1 and standard deviation 0.5) were convolved with the measured HRF at 0.08 s resolution, sampled at TR = 0.72 s for 1200 frames, and Hann-windowed amplitude spectra were averaged over 120 simulated subjects. Subject averaging: 4000 spectra were generated from Eq. (1) with parameters drawn from normal distributions with the Table 1 means and standard deviations of Wu et al. [1], clipped to physically admissible ranges, and averaged. Sensitivity: peak prominence was measured with SciPy find_peaks; elasticities were obtained by central differences of ± 10% in each parameter, and the change needed to halve the peak by root finding between 0.3 and 3 times the fitted value. Analyses used Python with NumPy, SciPy and Matplotlib.

Ethics and use of AI tools

The study used only published group-level results derived from publicly available, de-identified HCP data, collected with informed consent under protocols approved by the Washington University institutional review board. A large language model (Claude, Anthropic) assisted with numerical analyses, figure preparation and editing but all analyses and text were checked by the authors.

Data availability

No new data were generated. The digitized spectra and HRF, the fitted parameters and the analysis code are available at https://github.com/WeiL11/spertral-fit

Declarations

Competing interests:

The authors declare no competing interests.

Author Contribution

J.C.G. conceived the model and wrote the manuscript; T.-W.L. assisted with analysis; Z.D. provided data from the study by Wu et al. and Z.D. Y.G. and J.C.G. interpreted the data: all authors reviewed the manuscript.

Acknowledgements

This work was supported by National Institutes of Health grants R01NS129855 (Z.D.), R01NS113832 and R01NS078680 (J.C.G.). Data were provided in part by the Human Connectome Project, WU-Minn Consortium (Principal Investigators: David Van Essen and Kamil Ugurbil; 1U54MH091657), funded by the 16 NIH Institutes and Centers that support the NIH Blueprint for Neuroscience Research, and by the McDonnell Center for Systems Neuroscience at Washington University.

Data Availability

No new data were generated. The digitized spectra and HRF, the fitted parameters and the analysis code are available at https://github.com/WeiL11/spertral-fit

References

1. Wu, S. et al. A distinct second spectral peak in white matter BOLD signals: mathematical modeling, spatial distribution and age-related evolution. Scientific Reports (20026) (under revision)Preprint at (2026). https://doi.org/10.21203/rs.3.rs-10770821/v1
2. Li, M., Gao, Y., Ding, Z. & Gore, J. C. Power spectra reveal distinct BOLD resting-state time courses in white matter. *Proc. Natl. Acad. Sci. USA* 118, e2103104118 (2021).
3. Schilling, K. G. et al. Anomalous and heterogeneous characteristics of the BOLD hemodynamic response function in white matter. *Cereb. Cortex Commun.* **3**, tgac035 (2022).
4. Li, M., Newton, A. T., Anderson, A. W., Ding, Z. & Gore, J. C. Characterization of the hemodynamic response function in white matter tracts for event-related fMRI. *Nat. Commun.* **10**, 1140 (2019).
5. Gao, Y. et al. Myelination selectively modulates BOLD signal in white matter. *Preprint at.* https://doi.org/10.21203/rs.3.rs-6597153/v1 (2025).
6. Gore, J. C. et al. The balloon model revisited. *Preprint at.* https://doi.org/10.21203/rs.3.rs-11197888/v1 (2026).
7. Buxton, R. B., Wong, E. C. & Frank, L. R. Dynamics of blood flow and oxygenation changes during brain activation: the balloon model. *Magn. Reson. Med.* **39**, 855–864 (1998).
8. Obata, T. et al. Discrepancies between BOLD and flow dynamics in primary and supplementary motor areas: application of the balloon model to the interpretation of BOLD transients. *NeuroImage* **21**, 144–153 (2004).
9. Grubb, R. L., Raichle, M. E., Eichling, J. O. & Ter-Pogossian, M. M. The effects of changes in PaCO2 on cerebral blood volume, blood flow, and vascular mean transit time. *Stroke* **5**, 630–639 (1974).
10. Campbell, N. The study of discontinuous phenomena. *Proc. Camb. Philos. Soc.* 15, 117–136 (1909).
11. Carson, J. R. The statistical energy-frequency spectrum of random disturbances. *Bell Syst. Tech. J.* **10**, 374–381 (1931).
12. Rice, S. O. Mathematical analysis of random noise. *Bell Syst. Tech. J.* **23**, 282–332 (1944).

13. Wu, G. R. et al. A blind deconvolution approach to recover effective connectivity brain networks from resting state fMRI data. *Med. Image Anal.* **17**, 365–374 (2013).
14. Fultz, N. E. et al. Coupled electrophysiological, hemodynamic, and cerebrospinal fluid oscillations in human sleep. *Science* **366**, 628–631 (2019).

Figures

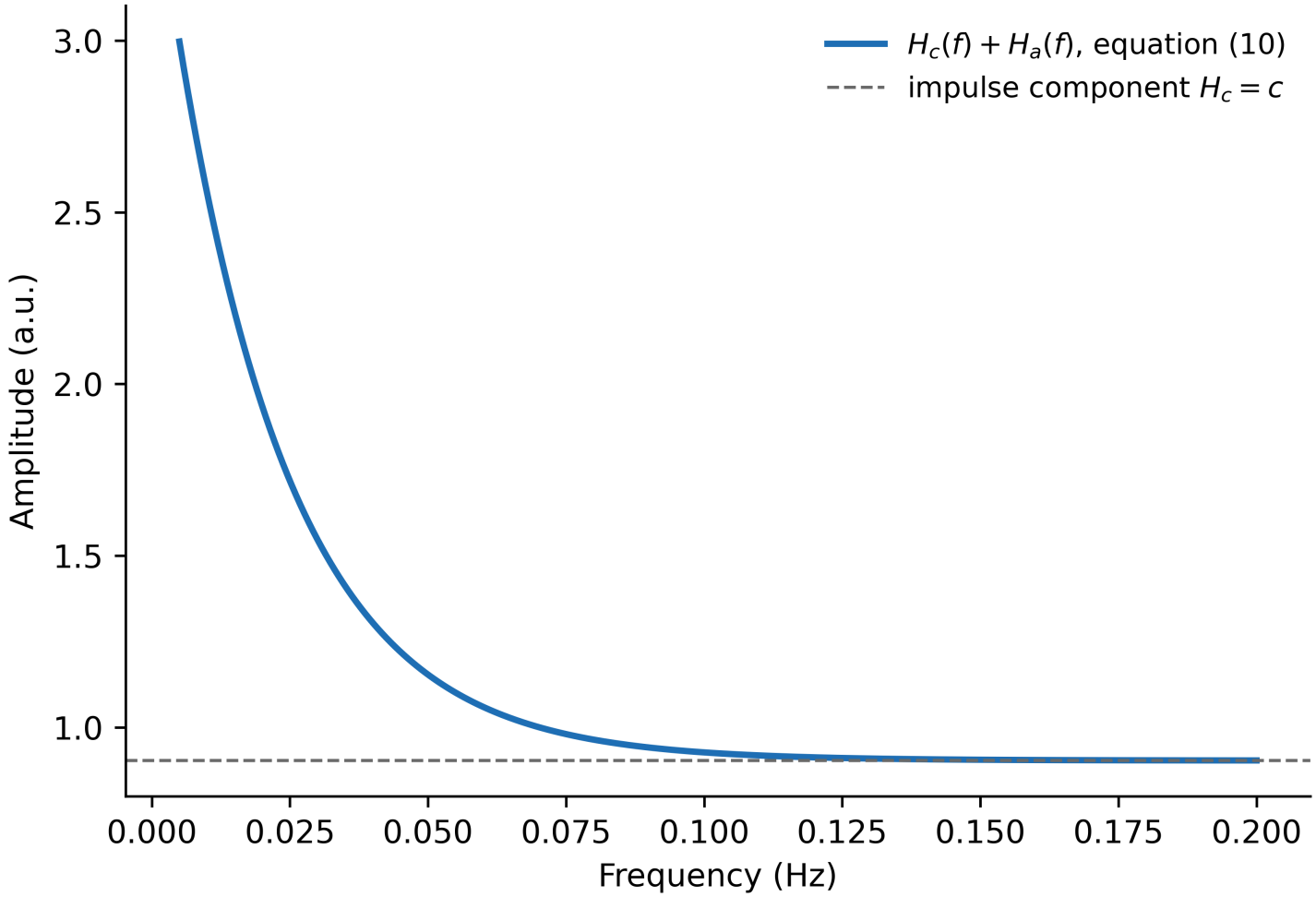


Figure 1

The neural input before hemodynamic filtering, H_c (f)+H_a (f) of equation (10), evaluated at the fitted floor and shoulder parameters. The curve is monotonic across the frequency range of the target spectrum: no resonance is possible from these two components alone.

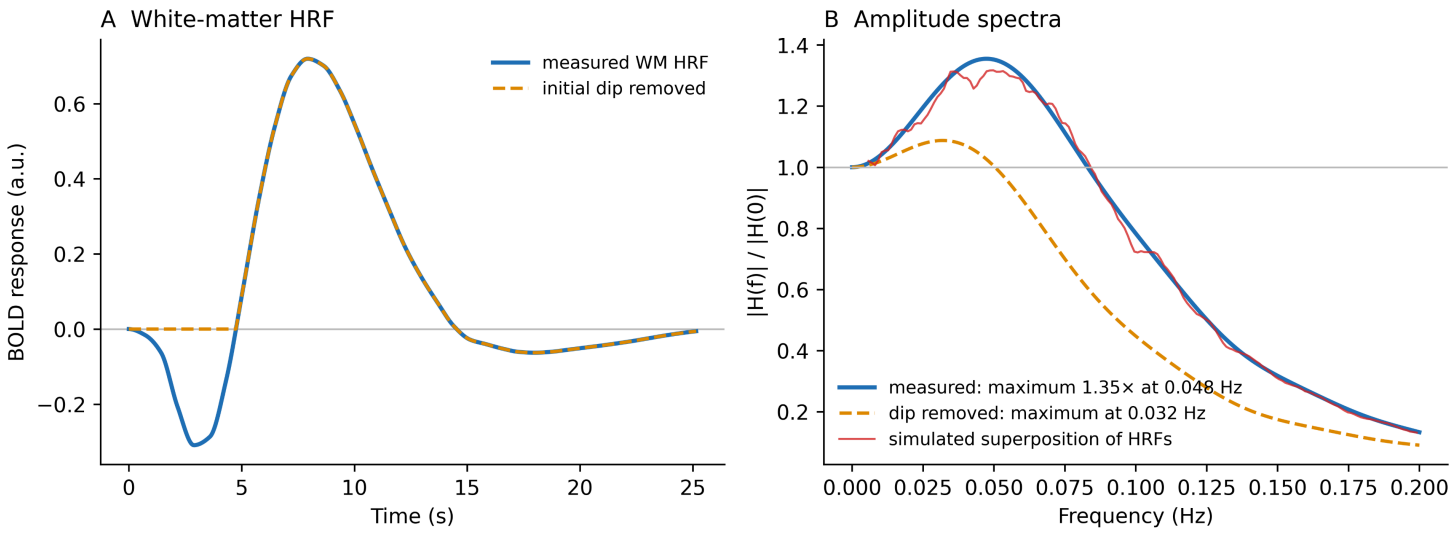


Figure 2

The white-matter HRF is a band-pass filter. Left: the population-averaged white-matter HRF of Schilling et al. [3], and the same response with the initial dip set to zero. Right: amplitude spectra of the two responses, normalized to their zero-frequency values, and the spectrum of a simulated superposition of randomly timed responses (thin line).

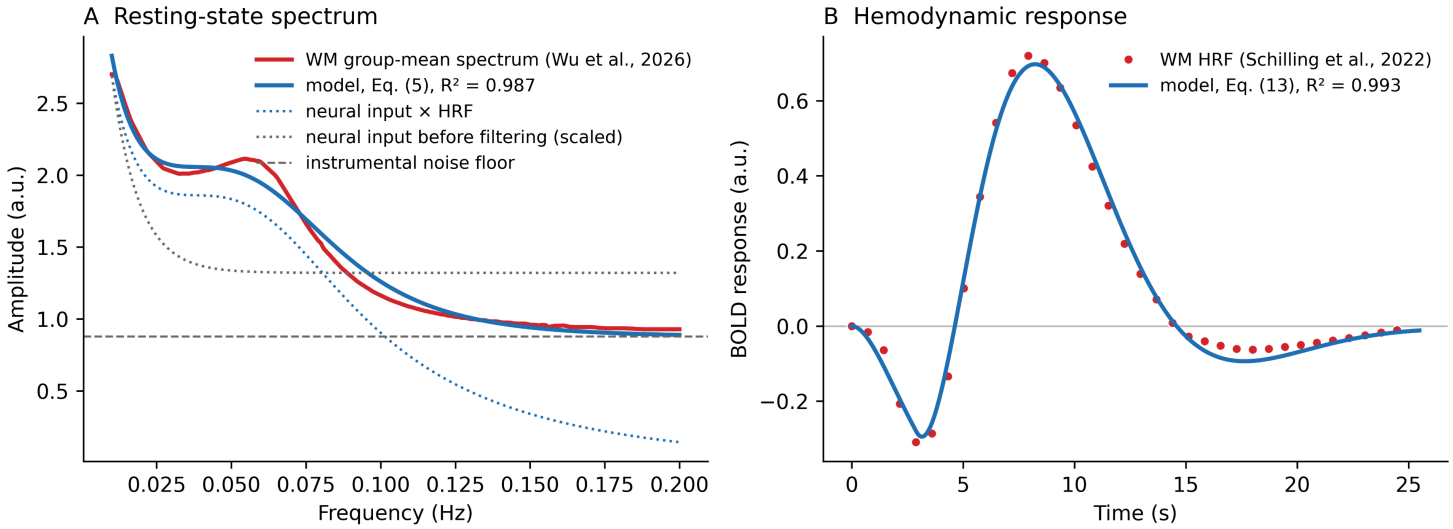


Figure 3

One set of hemodynamic parameters (equation (14)) fitted jointly to the resting-state spectrum and the HRF of white matter. Left: the group-mean white-matter spectrum [1] and the model of equation (5), with the neural input before and after hemodynamic filtering and the instrumental noise floor. Right: the white-matter HRF [3] and the impulse response of the same model, equation (13).

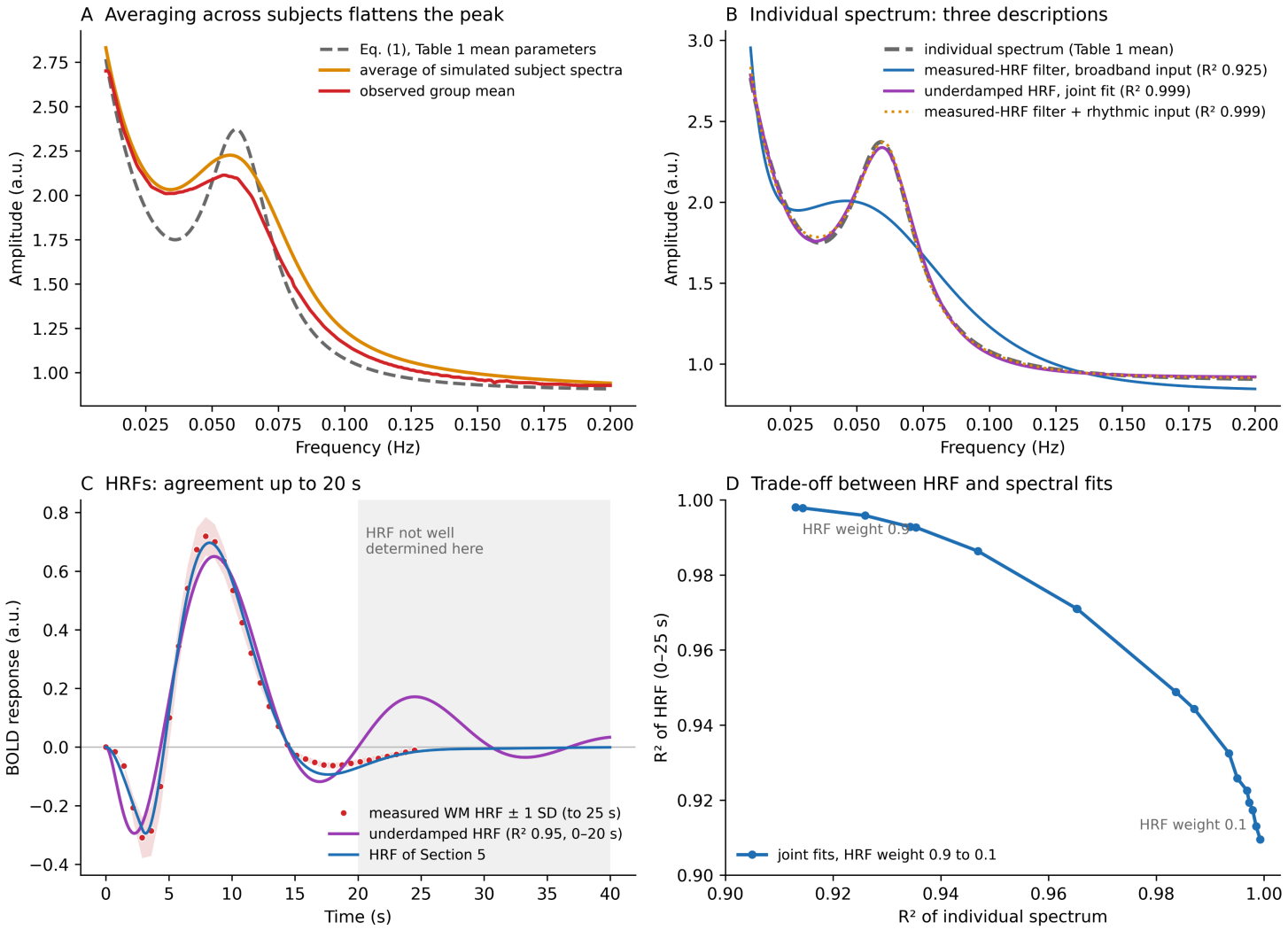


Figure 4

Group-mean and individual spectra. A: equation (1) with the per-subject mean parameters of Wu et al. [1] (Table 1), the average of 4000 simulated subject spectra with parameters drawn from the reported means and standard deviations, and the observed group mean. B: the per-subject mean spectrum and three descriptions of it: the jointly fitted HRF with a broadband input; an underdamped HRF fitted jointly with the measured HRF, with priority given to the spectrum; and the jointly fitted HRF with a rhythmic input component. C: the measured white-matter HRF ([3]; mean ± 1 SD across subjects, reported to 25 s), the underdamped HRF of panel B and the jointly fitted HRF; the shaded interval after 20 s is where the measured HRF is not well determined. D: HRF fit against spectral fit for joint fits with the weight on the HRF varied from 0.9 to 0.1 (HRF fitted over 0–25 s).

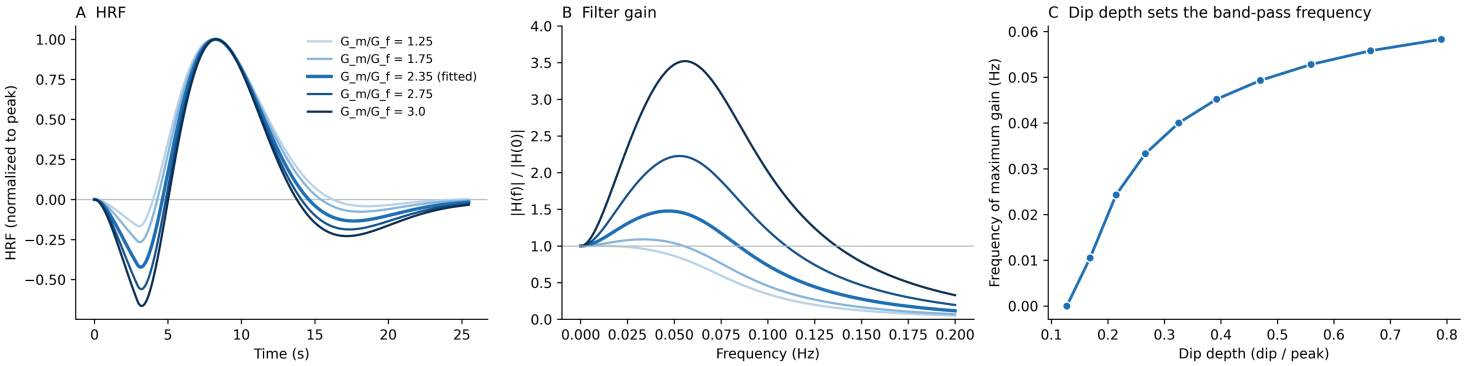


Figure 5

The metabolic weight links the dip to the spectral elevation. Left: impulse responses of equation (13) for Gm/Gf from 1.25 to 3.0, other parameters as in equation (14), each normalized to its peak. Centre: the corresponding filter gains, normalized to their zero-frequency values. Right: frequency of maximum gain against dip depth for Gm/Gf from 1.0 to 3.25.

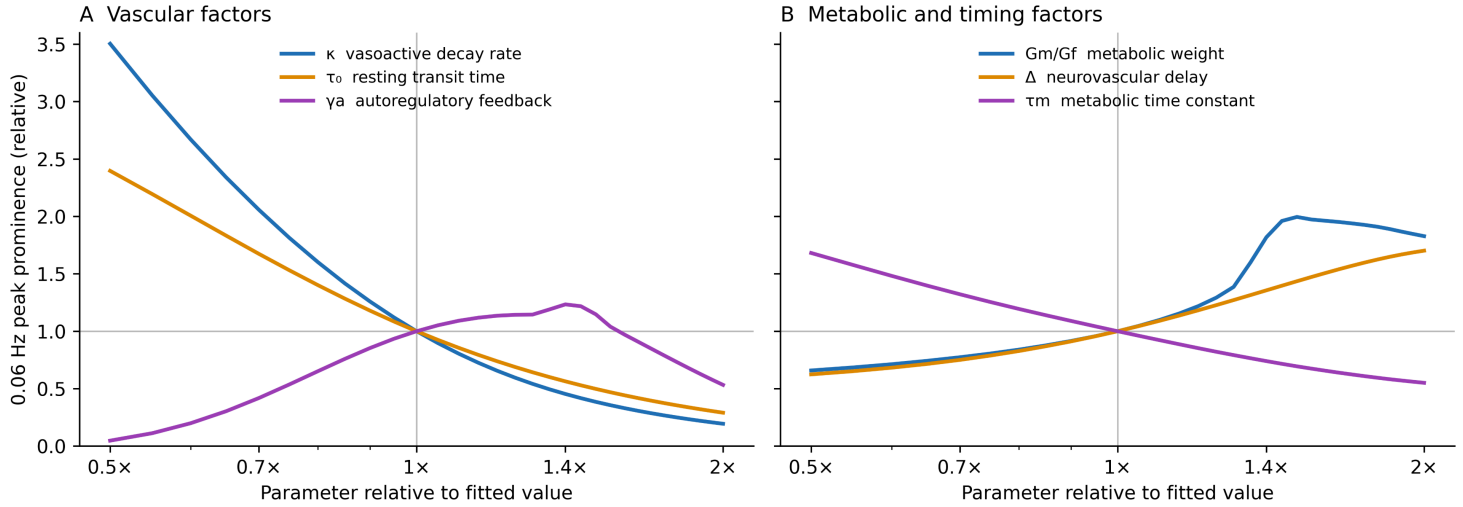


Figure 6

Sensitivity of the white-matter spectral peak to the parameters of the HRF. Each parameter was varied alone about its fitted value (equation (14)), with the rhythmic input fixed; the prominence of the spectral peak is shown relative to its value at the fit. Left: vasoactive decay rate κ, transit time τ0 and autoregulatory feedback γa. Right: metabolic weight Gm/Gf, neurovascular delay Δ and metabolic time constant τ_m.